Chapter 6
A Socio-Ecological Perspective on COVID-19 Spatiotemporal Integrated Vulnerability in Singapore

Chan-Hoong Leong, Wei Chien Benny Chin, Chen-Chieh Feng, and Yi-Chen Wang

6.1 Introduction

The global COVID-19 pandemic has impacted public health, economics, and political confidence in profound and complex ways. Singapore reported its first COVID-19 case on January 23, a visitor from Wuhan, as the source of the outbreak. The first Singaporean infected case was reported on February 4, involving a customer service assistant who worked at a retail shop visited by Chinese tourists who were carriers of the disease. By early March, local transmission clusters were reported at places of worship, entertainment outlets, and clubs. On April 7, the city-state was placed on a partial lockdown, locally coined as a "Circuit Breaker" (CB), to contain the viral transmission. Other than those in essential services such as healthcare, public sanitation, and energy providers, all workers must stop work or do so online. Eldercare and Senior Activity Centres were closed, and school lessons transited to home-based learning. The movement of people was curtained and strict social distancing rules were enforced to discourage interactions. Recreational facilities were closed, and restaurants could only offer take-away food.

At the start of the CB, a total of 1,481 COVID-19 cases, or a daily average of 50 to 100 cases, was reported in Singapore (Ministry of Health (n.d.)). The number of daily infections peaked at 1,426 new cases on April 20, with the majority from migrant workers' dormitories. By early June, the CB had seemingly broken the chains of infection as the number of daily infections declined, averaging less than 10 community cases a day, and about 200 to 300 cases a day in the dormitories. On June

C.-H. Leong (✉)
Singapore University of Social Sciences, Singapore, Singapore
e-mail: chleong@suss.edu.sg

W. C. B. Chin
Singapore University of Technology and Design, Singapore, Singapore

C.-C. Feng · Y.-C. Wang
National University of Singapore, Singapore, Singapore

S. Shaw and D. Sui (eds.), *Mapping COVID-19 in Space and Time*, Human Dynamics in Smart Cities, https://doi.org/10.1007/978-3-030-72808-3_6

2, schools were gradually re-opened (Phase 1 opening), and by June 19, the CB was partially lifted, where restricted forms of shopping, restaurant dine-in, office work, and recreational activities were permitted (Phase 2 opening). There were a total of 41,615 cases of COVID-19 infections as of June 19, 2020.

The evidence so far suggests that the disease spreads directly and indirectly from human-to-human contact. An infected person may pass on the virus to the next individual through the surface of an object that the person come in contact with, and more likely so if the latter touches the nose, mouth or the eyes. In contrast to past global epidemic like SARS, or MERS, COVID-19 is an airborne and highly virulent respiratory disease with long incubation period (Morawska and Milton 2020). Indoor venues, places with poor ventilation, and where people linger around longer are more prone to transmission (Lewis 2020). The stealthy and exceedingly contagious respiratory virus makes this disease a potential deadly strain.

Scientific knowledge in this pandemic is still limited, particularly how the types of social and built environmental attributes may contribute to epidemiological risk. The goal of this chapter is to develop a measure of spatiotemporal vulnerability in Singapore. Specifically, we use the data on movement restrictions from the COVID-19 outbreak to highlight how an epidemic may evolve over space and time due to the inherent risks to certain subgroups and the type of amenities that attract human congregation and transmission. The chapter will first give an overview on the socio-built environmental characteristics that are linked to community resilience and pathogenic infections, follow by a review on how temporal fluctuations in movement of people may shape local vulnerability. This study coalesces different data sources using demographic profiles, human mobility, and urban spatial functions to produce a new perspective and measure on spatiotemporal vulnerability.

6.2 Literature Review on Environment and Vulnerabilities

There is a historical curiosity to understand how a location is linked to human behaviours, motivations, and wellbeing, and by extension, the place's vulnerability to devastations from hazards. Policymakers, urban planners, disaster response management, and public health officials have a strategic interest to find out what are the social or built environmental features that can shape adaptation as this knowledge can provide the conduit to assess and predict disaster, and provide the foundation for prevention and recovery (Adger 2006; Cutter 1996; Cutter et al. 2003, 2008). Built features such as pedestrian friendly walkways, aesthetically designed corridors, and access to facilities are known to encourage increased mobility, social interactions, and community participation (e.g., Leslie et al. 2007); places with abundance of nature, vegetation, and sunlight are found to improve healing and rejuvenation from psychological distress (e.g., Bratman et al. 2012; McMahana and Estesb 2015).

Alternatively, social features such as a neighborhood's demographic profile on age, income, density, and racial composite, give policymakers insights on potential areas that are susceptible to socio-economic disruptions, experience higher risk to

mental and physical health, or face greater impediments to post-disaster recovery and humanitarian aid. The Social Vulnerability Index (SVI) developed by the US Centers for Disease Control and Prevention (CDC) demonstrates how information about the social environment is harnessed to identify vulnerable locations and where the deployment of emergency shelters are needed most (e.g., Flanagan et al. 2018). SVI composes 15 US census tract indicators, covering four demographic and geographical attributes, namely socio-economic status, household composition, minority status, housing and transportation. Overall, locations with a higher concentration of elderly, minority races, and lower income households are predisposed to greater vulnerability.

Recent evidence from the US and Europe on the COVID-19 outbreak corroborated this observation. Places that are densely populated, with more senior citizens, young children, non-whites, working class residents, and people with pre-existing medical conditions reported a higher infection rate and mortality compared to middle-upper class neighborhoods (e.g., Karaye and Horney 2020; Mueller et al. 2020; Nayak et al. 2020; Snyder and Parks 2020; Yonker et al. 2020). The findings reflect the conflation between race, class, and occupational hazards, as more minorities live in disadvantaged estates, employed in lower-paying occupations, lack access to healthcare, and medical insurance. Social vulnerabilities are a product of structural socio-economic inequalities, and their disabilities are amplified during a crisis, with the least resources to cope with the ensuing disruptions (Cutter et al. 2003).

Last but not the least, the conceptual framework on spatial vulnerability to pandemics has helped informed locale emergency management, including heat-related injuries (Lehnert et al. 2020), floods (Rufat et al. 2015), and earthquakes (Schmidtlein et al. 2011). Notwithstanding these contributions, many of the spatial vulnerability indicators are static and time-invariant. It does not capture the dynamics of human mobility, which has a temporal and class dimension attached. In other words, the risk changes across space and time. The COVID-19 outbreak is also different from previous epidemics in a few significant ways. First, there is a greater recognition and practice of heath preventive measures such as safe distancing, work from home, and travel restrictions. Specifically, young children, elderly, and those with medical conditions are confined at home during the early stages of lockdown to minimize interactions.

Second, COVID-19 is considerably more infectious than the previous known diseases such as SARS and MERS (Petrosillo et al. 2020). The lessons learned from the SARS pandemic, such as isolation of suspected and confirmed cases, are considerably less effective this time. Exposure to the infectious disease, specifically in places or Point of Interest (POI) where people congregate remain the crucial determinant that underscores transmissions. These include supermarkets, shopping malls, and public transportation nodes. The centrality (i.e., intensity of linkages to other locations/nodes) and transitivity of locations (i.e., clustering with other locations that are also directly linked up between them) predicted the severity of infections. This pattern of transmission is also reflected at the regional level. Studies on the Black Death plague for instance, found that cities that are major intersection networks are significantly more vulnerable (Gómez and Verdú 2017). Proximity to spatially

vulnerable POI and networks of densely connected nodes increases the probabilities of local infections (Bogich et al. 2013; Tatem et al. 2006).

Third, there is a pungent public discourse on socio-economic inequality in the COVID-19 pandemic (Schwirtz and Cook 2020). Most of the higher income earners, the professionals, managers, and executives, can performed their job remotely, i.e., work from home. Conversely, those employed in provision of essential services, such as public transport, postal and food delivery, building maintenance, energy providers, law enforcement, and water and waste management services, still have to commute to work daily and exposing themselves to the risk of infection. This narrative is not unique to Singapore. Similar debates can be heard in other infected countries. Taken together, the evidence suggests that a lockdown may have dissimilar spatiotemporal impact to people from different socio-economic background. In addition, due to the compact nature of city-states like Singapore, we expect the overall risk to be affected by both local and proximity effects. Specifically, neighboring areas that are considered vulnerable will have a spill over impact on local residential risk.

In summary, it is important to develop an Integrated Vulnerability (IV) model to address geographic variation on risk assessment and disruption according to the CB timeline (i.e., lockdown) in Singapore. This variability is a consequence of resource inequality across space that is dynamic but highly influential in light of the virulent nature of COVID-19. Residential areas with disproportionately more vulnerable residents (i.e., young and elderly residents), low income families (using housing prices as surrogate), concentration of POIs/amenities and built features known to attract human congregation and disease transmissions (e.g., public transportations, markets) will have a higher spatial vulnerability. In line with expectations from network theory where higher concentrations of centrality and transitivity accelerated pandemic outbreaks, neighborhoods that are contiguous to other estates with similar spatial vulnerabilities will likely produce a higher risk than remote, dis-contiguous areas with limited exposure to the hazardous POIs (i.e., spatial lag effect). Spatial vulnerabilities however will change in line as the rules governing CB change over time, as more business, work, and school activities gradually resume prior to the lifting of the lockdown.

6.3 Data and Method

The measure of IV to COVID-19 is segmented by monthly data and using subzone as the basic enumeration unit. Singapore is a compact island city-state with an area of 720 km^2, and a population of five million people, including long-term and transient residents. A subzone is the smallest zonal unit used in urban planning. It is commonly centered around a focal point like a neighborhood center[1]. There are 323 subzones with varying sizes, population, land use, and demographic profiles. Demographic

[1]About 10 subzones make up a planning area, a broader division of regional towns with about 70,000 to 100,000 residents.

data for a subzone can be obtained from Singapore Department of Statistics (www.singstat.gov.sg). The data includes the configuration of housing types, and population segmented by gender, race, and age. The map representing all subzone divisions and its demography showing population density and the proportions of young, working age adults, and elderly residents can be found in Fig. 6.1.

Monthly data on public transport utilization and housing resale prices is used (Table 6.1). The former shows travel pattern among commuters of buses and trains and is obtained from Ministry of Transport, Singapore. Majority public transport commuters rely on a store-value card when using the transport system. The points of entry and exit in each train station or bus stop are registered in a national transport database, and the consolidated data reflects the intensity of human activities in the various subzones. This movement elevates the risk of COVID-19 transmission as the virus is known to spread from human to human in close proximity.

Housing resale prices are obtained from the Ministry of National Development. This data includes all property transactions over a three-year period between 2017 to 2019. More than 9 in 10 properties in Singapore are apartments co-located in the same block sharing the same postal code. Less than 10% of all properties are

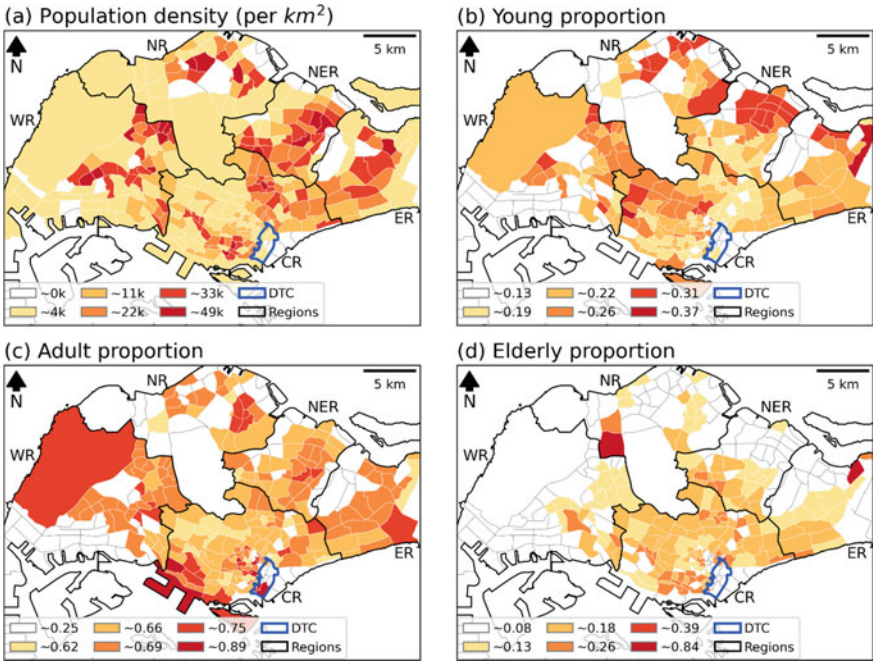

Fig. 6.1 Map of Singapore representing **a** population density, **b** proportion of young residents (age 19 and below), **c** proportion of adult residents (between age 20 and 64), and **d** elderly residents (age 65 and above). The polygon in blue shows the Downtown Core, which constitutes the bulk of the Central Business District. WR, NR, NER, ER, and CR, represent Western region, Northern region, Northeast region, Eastern region, and Central region, respectively

Table 6.1 Spatial and temporal information used in this study

Category	Details	Static/dynamic
Demographic	Population in each subzone, segmented by 5-age-interval	Static
Public transport flow	Number of passengers from one bus-stop/train-station to another	Dynamic
Residential	Resale housing prices by building blocks	Static
Facilities POI	12 types of POI, classified under four amenity categories: – commercial: shopping malls (199), supermarkets (324), wet markets/hawker centers (114); – transportation: train stations (183), bus interchanges (48), bus stops (5,045); – facilities: sport facilities (182), medical facilities (54), community clubs (112) – other: worship places (654), coffee shops (1,136), community in bloom parks (1,024)	Static
Urban planning	9 categories: residential, business/commercial, agricultural, transportation, education, health/medical, religious, public open space, and other	Static

classified as a landed unit (i.e., own a plot of land), some of which have its own postal code or sharing one with a handful of other dwellings. The average transaction price for each postal code is computed. This data serves as surrogate on socio-economic status, where a higher average transaction price reflects middle-upper class, and vice versa.

To evaluate the land use mixture of each subzone, the data on land use categories was extracted from the Singapore Master Plan 2019 provided by Urban Redevelopment Authority of Singapore. The original data came in Keyhole Markup Language (kml) format, which contains detail polygons of building blocks, street profile, etc., and a column of land use description for each polygon. A total of 33 land use descriptions were provided, which contained subdivisions of some major land use categories or a mixture of them (e.g., business, residential and residential with commercial on first storey).

6.3.1 Data Pre-processing

The obtained data was converted to subzone-based attributes and unit interval values for the calculation of local risks. There are six measures in each subzone, including population density (PD_i), elderly population density (ED_i), property resale transactions (PT_i), accessibility of subzone (Acc_i), land use diversity (LE_i), and population activity intensity (IF_i).

6.3.1.1 Demographic and Socio-Economic (PD_i, ED_i, PT_i) Data

Two demographic aspects were included in the measurement of local risk—population density (PD_i) and elderly density (ED_i). The total subzone resident population and elderly population (age 65 and above) were divided by the area size to obtain the two density values for each subzone. The two population density values were converted to unit interval using their minimum and maximum values. We used the average housing resale price to capture the socio-economic aspect of each subzone. For those subzones with no housing resale data, a simple estimation based on 10 nearest neighbors and weighted by the spatial distance was performed. The property transaction value for each subzone (PT_i) was calculated as the natural logarithmic of the (estimated) average resale price, with a conversion to unit interval using the minimum and maximum values.

6.3.1.2 Measurement of Accessibility (Acc_i)

This study used potential accessibility to some commonly utilized facilities to capture the possibility of viral exposure. In total, 12 types of POI were included, classified under four amenity categories (Table 6.1). The number of POIs for each type varies considerably. There are nine facility types with less than 1,000 POIs each, these include medical facilities (54), train stations (Mass Rapid Transit (MRT)/Light Rail Transit (LRT), 183), bus interchanges (48), sport facilities (182), supermarkets (324), wet markets and hawker centers (114), shopping malls (199), places of worship (churches, Chinese temples, mosques, and Hindu temples, a total of 654), and community clubs (112). There are three facility types with more than 1,000 POIs each, namely bus stops (5,045), coffee shops (National Environment Agency, 1,136), and community in bloom parks (1,024).[2]

For the first group (i.e., less than 1,000 POIs in each type), because of limited accessibility, residents must go to the nearest facility to access the specific function, such as healthcare or transportation. Thus, for each of these facility types, we calculated the accessibility (Acc_i^k) as the natural logarithmic of the inverse square distance from each subzone centroid (i) to the nearest facility of the specific type (k), or in mathematical form: $ln((dist_i^k)^{-2})$. For the second group, these facilities are more accessible island wide; residents have options if they need to use the specific utility. Thus, for each of these facility types, we count their number within a subzone and compute the natural logarithm of the count as a measure of accessibility, or in mathematical form: $ln(\text{count}_i^k)$. For each subzone, the 12 accessibility values are scaled to unit interval using the minimum and maximum values of each facility type, and the arithmetic mean of the twelve scaled values is used as the integrated accessibility (Acc_i).

[2] A "coffee shop" is colloquial term that refers to a place that offers dine-in food, drinks and a place where people gather to interact.

6.3.1.3 Land Use Diversity (LE_i)

Land use diversity measures the mixture of activities in each subzone. The data on 33 land use descriptions was categorized into nine major land use types (including residential, business/commercial, agricultural, transportation, education, health/medical, religious, public open space, and other) for analysis. For each subzone, the area for each of the nine land use types was calculated and integrated into a diversity measurement (LE_i) based on the Shannon's entropy equation (Shannon 1948), and normalized using natural logarithmic of nine. The normalized entropy values range within unit interval.

6.3.1.4 Population Activity Intensity (IF_i)

The subzone demographic data reflects the residential population and where they live, but not where they work or study. To capture the daily activity of the population, we included a measure of public transport utilization, specifically the incoming flow of bus and train users as a surrogate index of the population activity intensity. Figure 6.2 shows the daily average number of trips for trains (including MRT and LRT) and buses from December 2019 to July 2020, as a reference to understanding the changes in commuting patterns in Singapore during the COVID-19 epidemic. At the start of the global outbreak in February and March, there is a significant drop in weekend trip counts as residents reduce non-essential outdoor activity to minimize social interactions. The CB was implemented on April 7 and lasted till June 2. Public commuting activity for both weekdays and weekends dropped significantly in the

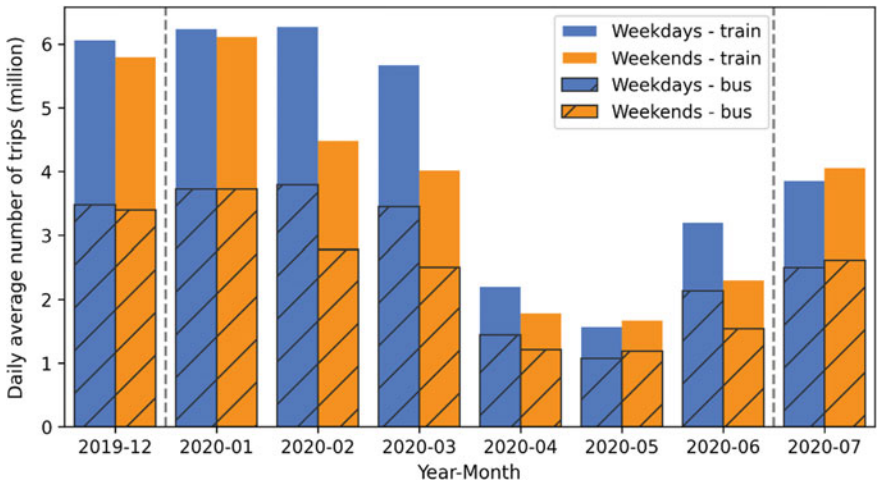

Fig. 6.2 The daily average number of trips for trains (MRT and LRT) and buses from December 2019 to July 2020

months of April and May. The first two phases of reopening took place on June 2 and 19, respectively. By the end of July, the number of trips was still considerably lower than usual compared to January data. We used the weekdays' incoming flow to a subzone as a surrogate variable to measure the population activity intensity in each subzone (IF_i). The incoming flows were converted into unit interval using the minimum and maximum values throughout the six months so that the resulting values were comparable between months.

A local vulnerability measure (LR) is first defined based on a non-weighted aggregate of local attributes in each subzone, e.g., demographic profile, socio-economic status, accessibility to facilities, land use, and population activity intensity. Population activity intensity assesses the number of people coming into each subzone. LR also incorporates POIs known to have high infections, such as shopping malls, supermarkets, and popular wet markets. Demographic profiles, socio-economic status, accessibility to facilities, and land use indicators are static and time invariant, activity intensity however fluctuates over the period when the lockdown was initiated, to the different phases of reopening.

$$\mathbf{LR_i} = \frac{1}{6}(\mathbf{PD_i} + \mathbf{ED_i} + \mathbf{Acc_i} + \mathbf{LE_i} + \mathbf{PT_i} + \mathbf{IF_i})$$

6.3.2 Metric of Spatial Lag Vulnerability

Spatial lag effects of vulnerability comprised two distinct components. First, the transition of the vulnerable effects due to human mobility. As the pandemic is transmitted primarily through human contact, the movement of people across space has implications to vulnerability, and proximity to active subzones and places with higher local risk would contribute to greater IV. Second, the spatial lag effects may differ for different groups of people. Working age adults in particular, are more mobile and subzones with a higher proportion of working age adults would have a higher transition of vulnerability.

6.3.2.1 Transition of Vulnerable Effects

The spatial lag effects are observed as the transition of elements from one place to another as a result of population flow (Fig. 6.3). In normal conditions (Fig. 6.3a), where there is no restriction of movement, population flow follows the gravity or radiation model of human movement patterns, both leading to an intense flow of people between neighboring subzones. Subzones with intense interactions would have greater likelihood of cross infections, and thus the condition of one location may be transferred to its neighboring subzones. During the CB period, the movement of people and interactions between places that were further apart were restricted

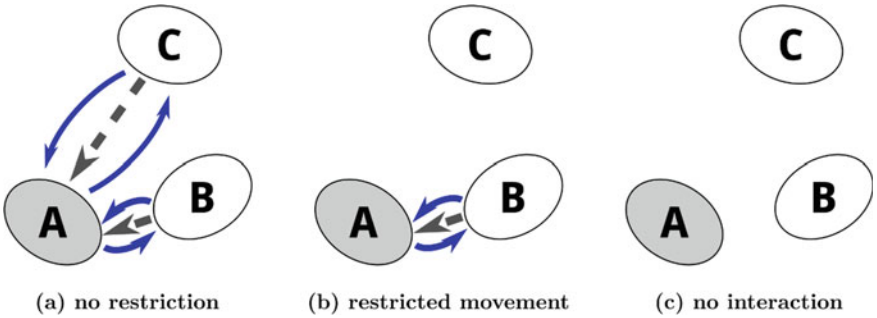

Fig. 6.3 An illustration on the transition of vulnerability between neighborhoods A, B, and C, with A as the target location: **a** no restriction, thus strong transition (dashed arrows) occurred with intense human exchanges (blue arrows); **b** when long distance movement is restricted, only residents in nearby neighborhoods have interactions with A, hence the shorter distance which contributes to the transition of vulnerability from B to A; and **c** when the CB in placed, no one is allowed to move across regions, hence zero transition

(Fig. 6.3b) or completely cut off across zonal boundaries (Fig. 6.3c). The analyses thus aimed to capture the transition of vulnerability, incorporating the spatial lag effects due to proximity and zonal contiguity.

6.3.2.2 Movements of Different Group of People

During CB, only providers of essential services are permitted to travel. This analysis examines the spatial lag effects of different age groups according to their IV exposure. The resident population was categorized into three age groups: young (19 and below), working age adults (20 to 64), and elderly (65 and above). The frequency distributions of the subzones by age groups are shown in Fig. 6.4. Most of the subzones have about 66.1% of working age adults, 20.5% of dependent young residents, and 13.5% of elderly residents. Since the working-age adults are expected to be economically active and spatially more mobile than both young and old residents, the potential transition of vulnerability caused by adult people would be greater than the other two age groups.

Figure 6.5 illustrated the different spatial lag effects of varying movement restrictions for different age groups in hypothetical scenarios. Under normal circumstances, everyone is free to move around, but most people tend to move within a distance range for their daily routines. In Fig. 6.5b, we assume everyone can move freely without restrictions and for any distance. During the early stage of the outbreak (Fig. 6.5c), the elderly is considered the most vulnerable group because their higher mortality rate; they were advised not to travel long distances and avoid crowded places. When the schools were closed (Fig. 6.5d), the younger residents were confined to home-based learning and hence zero distance travelled. Under a CB (partial lockdown) (Fig. 6.5e), most people are not allowed to leave their home except for essential workers. Under

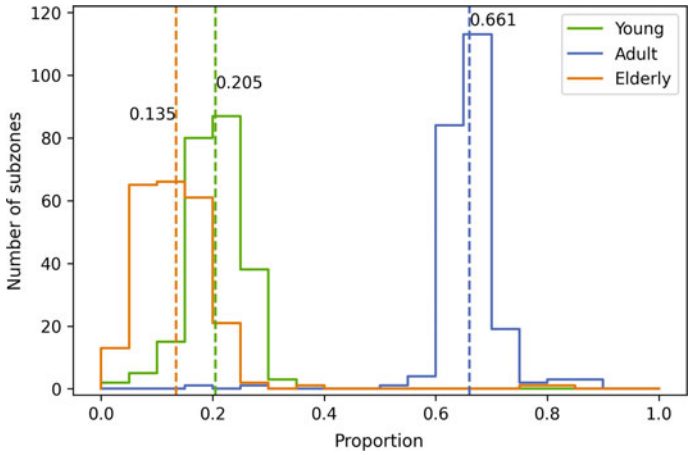

Fig. 6.4 The proportion of the three age groups in subzones. The values adjacent to the three colored dashed lines show the average proportion of the corresponding age group

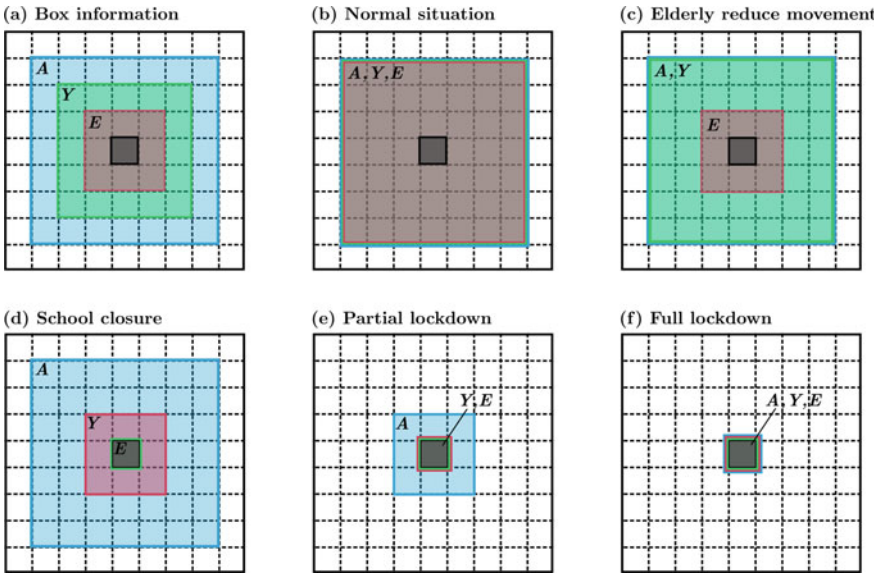

Fig. 6.5 An illustration of the transition effects by multiple age-group as a result of different restrictions and mobility between age groups: **a** The target location (dark gray), shows the moving distance for elderly (red, labelled with E), for working adults (blue, labelled with A), and for young students (green, labelled with Y); **b** to **f** indicates the transition effects of the three age groups from the varying neighboring distance to the target location

a full lockdown (Fig. 6.5f), no one is allowed to cross zonal boundaries, and the effects of neighboring areas would be zero.

For each age group (G), the spatial lag of vulnerable for a subzone *i* (Lag_i^G) is calculated with the following equation, which multiply the proportion of the respective population to total population ($prop_i^G$) with the average local risk of its neighboring subzones for the age group (using the neighboring weight $W_{i,k}^G$, which is 1.0 if the distance between two subzones is less than or equal to the moving distance for the age group, otherwise zero). Note that the spatial lag would have different neighboring weights ($W_{i,k}^G$) for different age group (young, adult, elderly).

$$Lag_i^G = prop_i^G \mathbf{x} \frac{\sum_k (W_{i,k}^G \times LR_k)}{\sum_k W_{i,k}^G}$$

where subscript *i*, subscript *k*, and superscript *G* represent a subzone, the contiguous subzones, and age group, respectively. Following this, we integrate the spatial lag effect in the computation of an IV index. For each subzone, the IV index:

$$IV_i = p(LR_i) + (1-p)\left(Lag_i^{elderly} + Lag_i^{adult} + Lag_i^{young}\right)$$

The IV in the equation reflects the vulnerability of a location; it is a function of its local risks (LR_i), and the neighboring vulnerability conditions. Local and neighborhood conditions however pose different impact on overall vulnerability, and this depends on the strength of their effects. There is a *p* parameter, representing the strength of effects from local environment, and $(1-p)$ represents the strength of effects from the neighboring subzones. Thus, a p-local value of 1.0 demonstrates complete local effect, no spatial lag; a p-local value of 0 demonstrates complete neighborhood effect, i.e., vulnerability is affected by characteristics of contiguous subzones.

6.3.3 Study Design

To explore the IV of disease outbreaks in Singapore and the effects of the parameters (moving distances for varying groups and the local effect), the monthly scenario analysis and sensitivity analysis were performed.

6.3.3.1 Monthly Scenario Analysis

In this section, we analyzed the travel patterns of Singapore residents from January to June of 2020, and provided an outline on the model assumptions for LR, spatial lag models, and IV. Table 6.2 shows the parameter configurations. In January, when the first few imported cases were identified, all moving distances were set to 25 km,

Table 6.2 The parameters configuration for the monthly scenario analysis

Month	p-local	Distance-young (km)	Distance-adult (km)	Distance-elderly (km)
January	0.5	25	25	25
February	0.5	20	25	10
March	0.5	10	25	10
April	0.25	0.5	25	0.5
May	0.2	0.5	25	0.5
June	0.35	10	25	10

a large enough radius that covers most of the subzones, signifying no restriction of movement. In February, and in light of many unlinked community cases (i.e., unknown sources of transmission), the government issued advisories against unnecessary outdoor events and traveling, and thus the reduction in the moving distance of the elderly and young residents.

The rapid increased of cases in late March led to the CB in April and May, and this restricted the mobility of young and elderly people. Only a short commute to the neighborhood grocery stores and food centers were allowed, and thus the travel distance for the two groups was set as 0.5 km. The travel distance for working age adults was set to 25 km (non-restricted) as some of them are essential workers who provide critical services to the country. Although a significant reduction of travelling was observed, there were approximately 2 million trips recorded during the CB period, and hence the effects of spatial lag for this category of residents (i.e., working age adults) was assumed to be similar to January for April and May.

The partial lifting of CB began in early June, where some were allowed to go back to work and school, although the businesses and individuals were urged to restrict their outdoor activities and social gatherings, and to work from home as far as possible. For this period, the moving distance of young and elderly people was increased to 10 km. Prior to the CB, the p-local effect is set to 0.5, i.e., half of the vulnerability of a subzone depended on its own local risk conditions, and the other half from the neighboring subzones. During CB, the p-local was reduced to 0.25 (April) and 0.2 (May), as people were not supposed to leave their homes. The p-local increased to 0.35 for June, as Singapore gradually reopens. As aforementioned, the local risk for each subzone was assessed using six variables, and where five of them were static. Only one of them, the population activity intensity, was based on the monthly public transport flow data.

6.3.3.2 Sensitivity Analysis

The following sensitivity analysis tested the different distance parameters and adjusted the local effects (p) incrementally to understand how the IV index changes. We used only the January public transport flow data as the population activity intensity variable, because the flow patterns for January was more stable compared to

the other months. Since the population proportion of young and elderly are lower than the working adults, the effect of the changing distances for young and elderly is expected to be low. As such, we combined the two age groups to share a moving distance[3] parameter in the sensitivity analysis. The range of the parameters' settings is as follows:

- effect from local (p-local): 0.0, 0.25, 0.5, 0.75, 1.0.
- moving distance for adult: 50, 100, 500, 1,000, and 3,000 m.
- moving distance for young/elderly: 50, 100, 500, 1,000, and 3,000 m.

In a pre-analysis, longer distances for young, adult, or elderly (from 3 to 30 km) showed similar patterns as the 3 km, indicating less sensitive effects for a further distance. Therefore, we present the results for emphasizing the fluctuation in the smaller distance range.

6.4 Results

6.4.1 Spatial Distribution of Local Risk

Local vulnerability (i.e., no impact from contiguous or proximal subzones) for each subzone is assessed based on local demographic and socio-economic profiles, spatial accessibility to essential facilities, and monthly incoming flows as a surrogate index of population activity intensity. Figure 6.6 shows the spatial distribution of local vulnerability. The subzones were categorized into six groups using the same set of break values derived from Jenk's natural breaks method, using the local vulnerability values of all six months. The frequency distribution plots for the local vulnerability of all six months and for each month were presented in Supplementary Figure S1. Since most of the variables were static throughout the six months and only the local population activity intensity changed over time, the overall spatial distribution was similar between months. The distribution mainly reflects the distribution of residential population density. Thus, the southern and central part of Singapore where the Central Business District (CBD) is located had slightly lower values. The Central region has a low population and density. Previous study (Chin and Bouffanais 2020) which attempted to identify super-spreader and super-susceptible locations in Singapore also obtained similar and counter-intuitive results—the Central Region (the CBD of Singapore) contained less than expected super-spreader and super-susceptible locations. These results highlighted that while the CBD might be important in the disease control, the residential areas could also have high risk of disease spreading thus should not be neglected (Huang et al. 2019).

[3]Moving distance parameter for sensitivity analysis is different from Table 6.2 as it was meant to measure a more active radius of mobility and interactions.

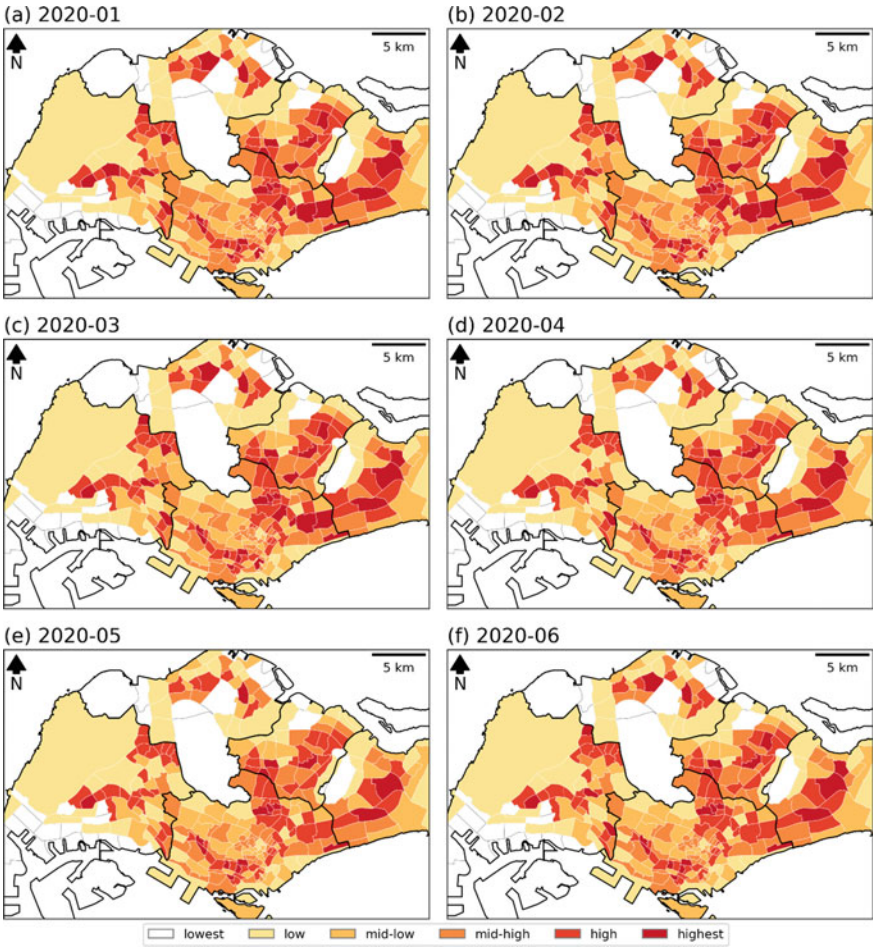

Fig. 6.6 Spatial distribution of local risk for the first six months. The local vulnerability values were categorized into six groups using a set of common break values (generated using Jenk's natural breaks method with all values stacked). Subzones with a darker shade are locally more vulnerable

6.4.2 Spatiotemporal Distribution of Vulnerability with Spatial Lag Effects

Using the aforementioned parameter settings, the effects of neighboring areas were included in the IV index for the six months (Fig. 6.7). Similar to Fig. 6.6, the subzones were categorized into six groups using the same set of break values derived from Jenk's natural breaks method and using the IV measures of all six months. The frequency distribution of the IV were presented in Supplementary Figure S2. The IV in January showed similar patterns with the local spatial vulnerability distribution (Fig. 6.6a). Most subzones in the southern part of Singapore, including the CBD,

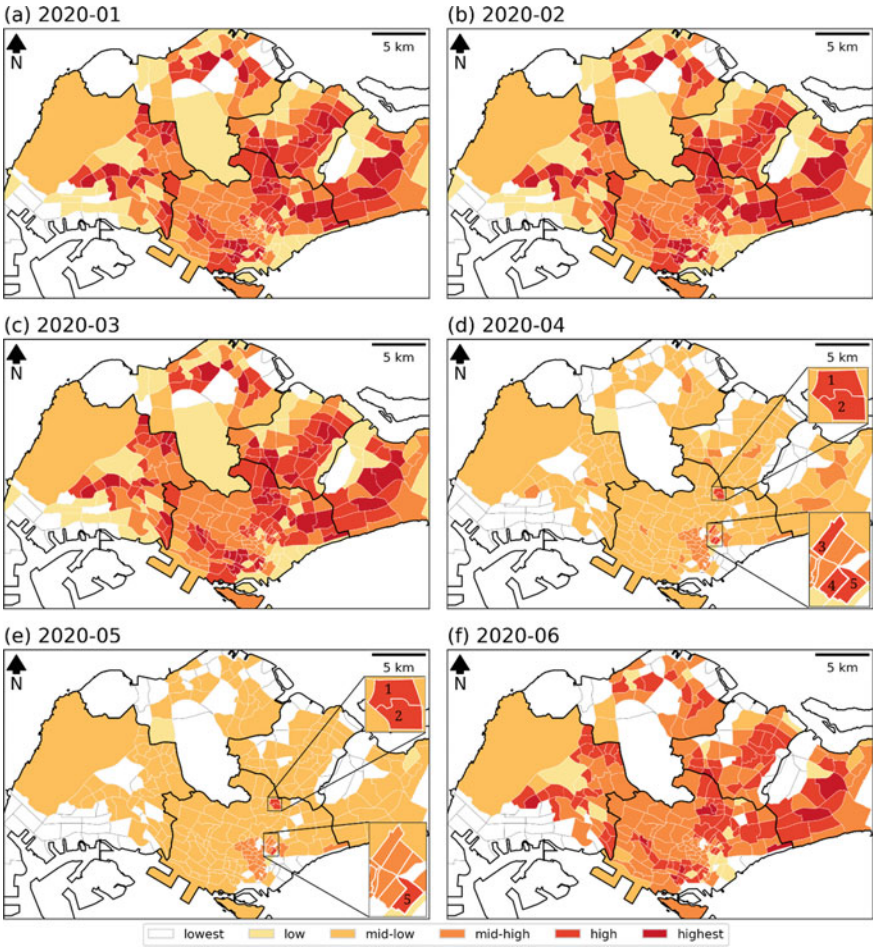

Fig. 6.7 Spatiotemporal distribution of the IV (local and spatial lagged) for the six months. The IV values were categorized into six groups using a set of common break values derived from Jenk's natural breaks method with all values stacked. A darker shade represents increased vulnerability. The highlighted subzones in (d) and (e) are: (1) Lorong 8 Toa Payoh, (2) Pei Chun, (3) Farrer Park, (4) Victoria, and (5) Bugis, respectively

where many of the businesses are located, have increment values from "lowest"-to-"mid-low", "mid-low"- to-"high". The relatively lower IV is partly due to the smaller population size and reduced density in this region. With the changes of spatial lag distances for elderly and young in February and March (reduced from 25 to 10 km), the spatial distribution patterns did not change. This may be attributed to the smaller representation of the two age groups (20.5% for young and 13.5% for elderly) in the population compared to the adult proportion (66.1%), leading to weak effects of reducing movement distance for the former.

During April and May, when the CB measures were implemented and most working adults were confined at home except essential workers, the IV of most subzones was reduced to level "lowest"-to-"low", with only a few subzones remained on level "mid-low"-to-"mid-high" (Fig. 6.7). Two subzones (Lorong 8 Toa Payoh and Pei Chun) remained at level "high" in April and May; Lorong 8 Toa Payoh's IV was level "high" for all six months, whereas Pei Chun's was on level "highest" on January to March, dropped to level "high" from April and June. Three subzones' IV ((3) Farrer Park, (4) Victoria, and (5) Bugis) also remained at level "high" for five months (from January to June except May); in May, only Bugis remained at level "high", while Farrer Park and Victoria dropped to level "mid-high". In other words, the measure to reduce moving distance for the five subzones was ineffective.

Figure 6.8a shows the changes in IV for each subzone over a six-month period. A clustering analysis of the trends based on k-means clustering with the Scikit-learn Python package (using silhouette score to determine the number of cluster-parameter k) was performed to identify the changes in IV for each subzone. Four distinct clusters were identified (Fig. 6.8b): In the first cluster, the IV values were similar for the first three months. After which, most of the scores declined in April, some of which accelerated down south to a trough in May (green, cluster-C). The second cluster demonstrated similar trajectory, albeit at a slower rate in May (blue, cluster-D). In June, the vulnerability values of most subzones began to pick up as the CB was partially lifted. The third cluster however, represents subzones that did not register a downward trend in April and May (red, cluster-A), i.e., consistently high. For the fourth and final cluster, the reduction rate was slower than the other subzones (orange, cluster-B). This indicates that the same moving distance restriction measures may have varying impact for different subzones.

Figure 6.9 shows the spatial distribution of the four clusters. Most subzones belong to cluster-C or D (blue or green), covering most areas of Singapore. All subzones of cluster-A (red) and cluster-B (orange) were in Central Region (Fig. 6.9b). Two subzones were classified as cluster-A (red cluster), including (1) Lorong 8 Toa Payoh and (2) People's Park. The IV slightly increased during April and May, which may

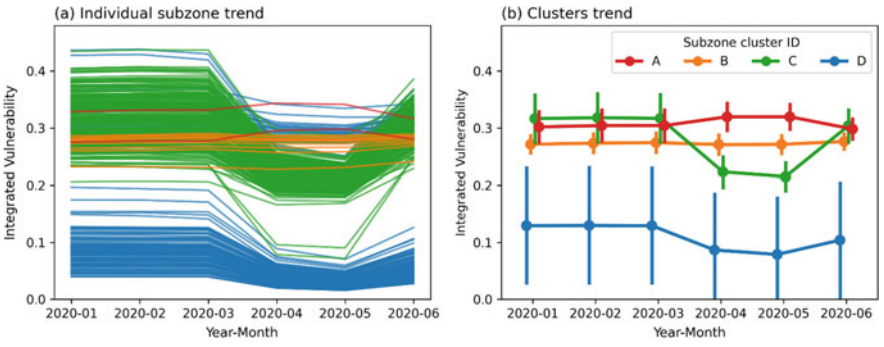

Fig. 6.8 Clustering results of the IV trend for subzones: **a** each line representing a subzone's IV, and **b** four clusters of IV for clustering of (**a**)

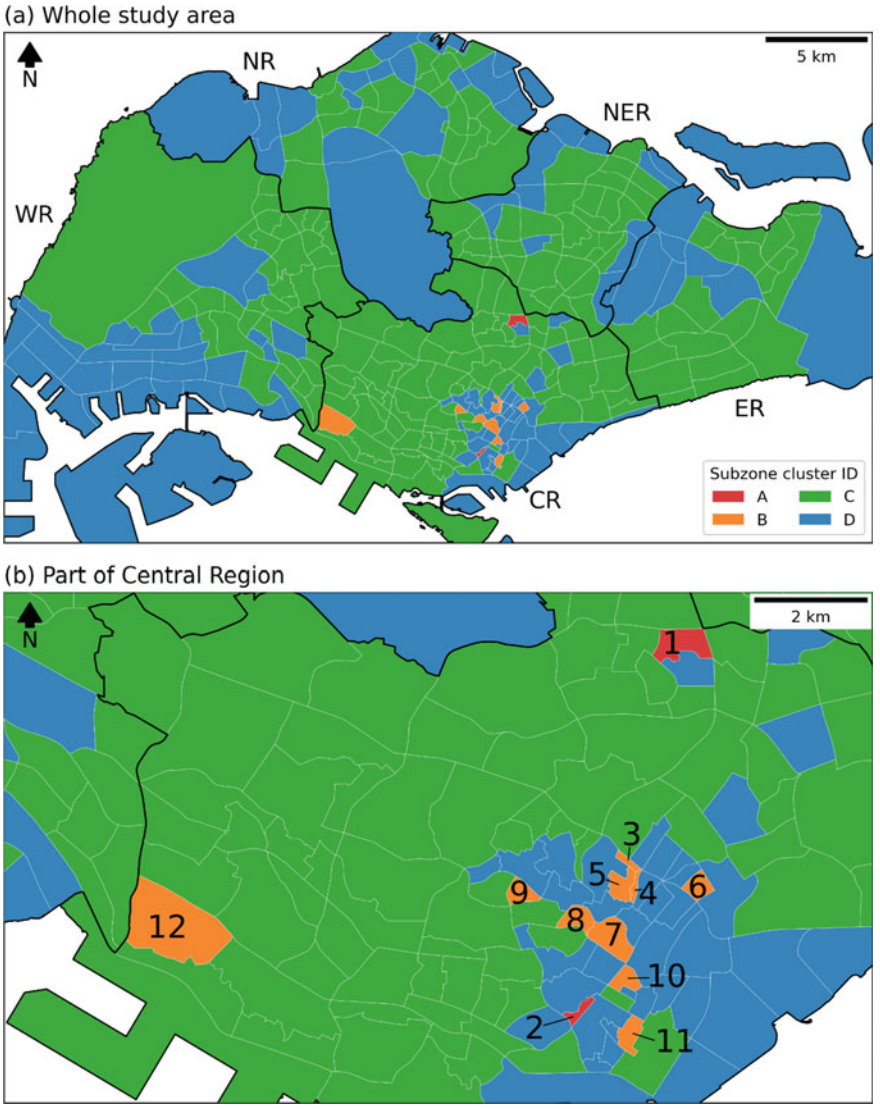

Fig. 6.9 Spatial distribution of the four clusters. The five regions of Singapore were labelled in (**a**): CR: Central Region, ER: East Region, NER: North East Region, NR: North Region, and WR: West Region. The subzones highlighted in the Central Region (**b**) are: (1) Lorong 8 Toa Payoh, (2) People's Park, (3) Mackenzie, (4) Selegie, (5) Mount Emily, (6) Kampong Glam, (7) Fort Canning, (8) Oxley, (9) Paterson, (10) Boat Quay, (11) Cecil, and (12) National University of Singapore

be a result of reduction in local effect (the parameter p), and increased neighboring effect (1-p), as the two subzones were surrounded by other subzones with higher local vulnerability. Ten subzones ((3) Mackenzie, (4) Selegie, (5) Mount Emily, (6) Kampong Glam, (7) Fort Canning, (8) Oxley, (9) Paterson, (10) Boat Quay, (11) Cecil, and (12) National University of Singapore) were classified as cluster-B (orange cluster). Almost all areas in the National University of Singapore subzone are used for education purposes, thus it contains low residential population, which implies level-low in local risk (Fig. 6.6). Alternatively, because of the low residential population, its IV was less sensitive to spatial lag effects, which was mainly based on the population proportions and distance settings, hence there was no reduction in April and May. The other nine subzones were located near the core area of Central Region. Each of the nine subzones has a small area size, and surrounded by other small subzones. In comparison to other areas, these subzones have a larger number of neighboring subzones in a given radius, and this leads to a relatively stable patterns and is less sensitive to the changes of moving distances parameters.

6.4.3 Sensitivity Analysis for Understanding the Effect of Restriction Distances and Local Proportion

Figure 6.10 shows the aggregated results for the combination of three variables, the effect from local (in the five subplots), the mobility distance for working adult (legend showing the lines with different colors), and distance for young/elderly (in horizontal axis). When local effect is set to 1.0 (Fig. 6.10e), i.e., effect from neighboring region is zero, the IV is fixed on the same value, and the distance for both adult and young/elderly would not have any effect. When p decreased to 0.75 (Fig. 6.10d), the IV started to decrease, with a gap appeared between the two lines with distance for adult set to 500 m and 1 km. The distance for young/elderly did not have significant effect when p set to 0.75. When p is set to 0.5 (Fig. 6.10c), which indicate half of the effect comes from the local, and half from its neighbors through the spatial lag effect, the IV will be significantly higher if the range of mobility is above 1 km across all age group.

In Fig. 6.10a, b, where the p parameter for the local effects were set to zero and 0.25, respectively (i.e., strong neighboring effect), the gaps in IV for the lines diverged, and the increment trends by the distance for elderly/young were most significant; in short, greater mobility range predicted higher IV. It should be noted that the standard deviation for the two figures is larger for the adult and elderly/young groups when the distance is set above 1 km and with a low value of local effect, meaning that the distributions were flatten and uncertainty is larger if the local effect is zero, i.e., IV is solely depending on its spatial neighbors.

These results highlighted the overall effects of the three parameters. Specifically, the proportion of local effect had a significant influence to the overall vulnerability; the impact from adult mobility distances appeared between 500 m to 1 km; and the

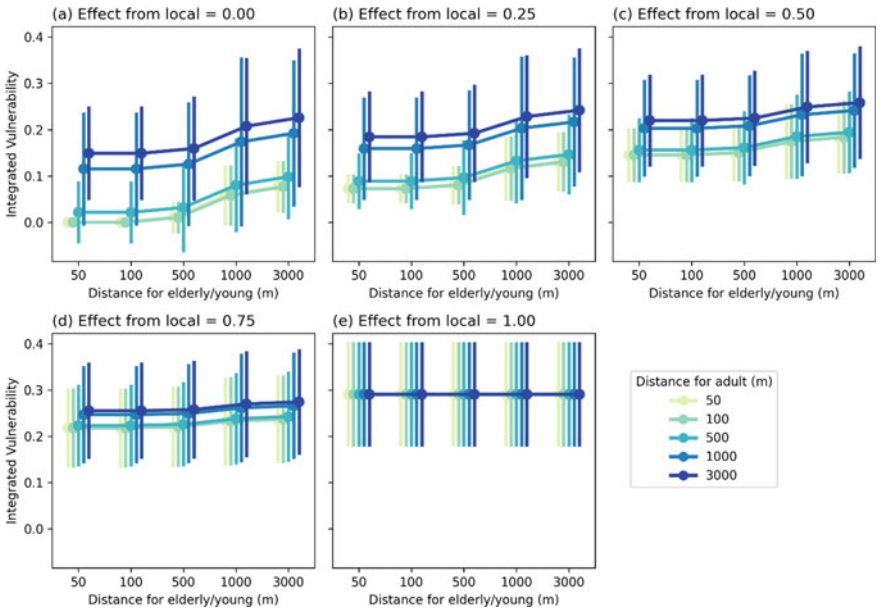

Fig. 6.10 Sensitivity analysis of the three parameters (local effects (p), distance for adults, and distance for young and elderly). The circle marker and error bars indicate the mean and standard deviation of all subzones for a given set of parameters

IV increases significantly if the distance for both adult or young/elderly is increased beyond 1 km. The details of the distributions were display in Supplementary Figure S3.

To find out the sensitivity of subzones' IV on adult mobility distances, we ran a k-means clustering with the lines of trends for each subzone by distance for young/elderly, segmented by the distance for adult (in individual subplot). The subzones with zero changes were filtered out from the clustering analysis (shown as cluster-F in Fig. 6.11). Figure 6.11 shows the clusters of trends by distance for young/elderly, which contained five clusters for each distance for adult parameters. Each cluster displays a unique trend by distance for young/elderly, which mainly occurs on the point of significant jump. For instance, where adult mobility is restricted to 50 m, cluster-C had an IV jump between 1 and 3 km; cluster-B increased between 500 m to 1 km; and cluster-A is seemingly most sensitive to travel distance of young/elderly, as it increased significantly between 100 and 500 m. The other two clusters (cluster-D and cluster-E) had low fluctuations, and the cluster-A is consistently higher than cluster-C. This means that the effect of distance for different subzone is also varied. In all other mobility radius (100, 500, 1,000, and 3,000 m), cluster-A has consistently demonstrated a significant leap wherever travel distance of young/elderly increased from 100 to 500 m.

The spatial distribution of the six clusters from Fig. 6.11 is illustrated in Fig. 6.12. Most subzones were either cluster F, cluster-C, or cluster-B. Cluster-A—seemingly

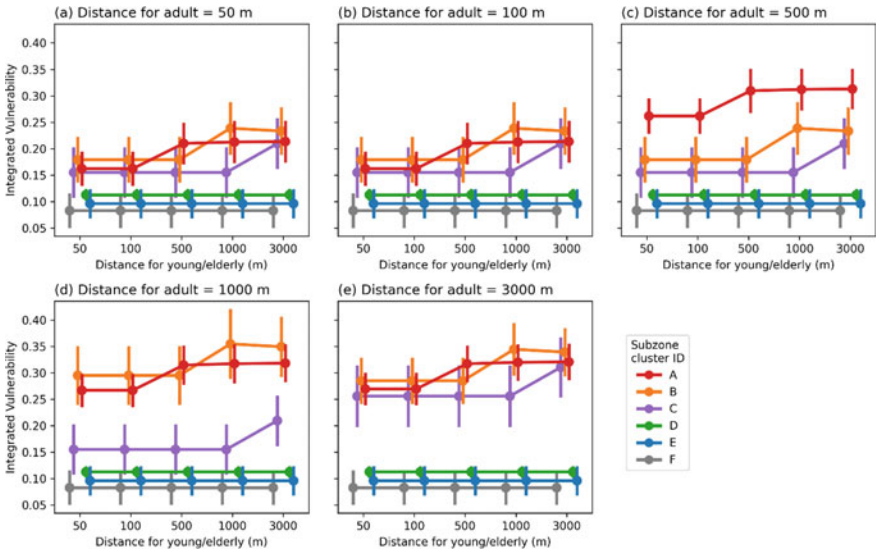

Fig. 6.11 Comparison of the effects of distance restrictions for adult versus young and elderly, with local effect (p) fixed at 0.5. Each color indicates different trend cluster

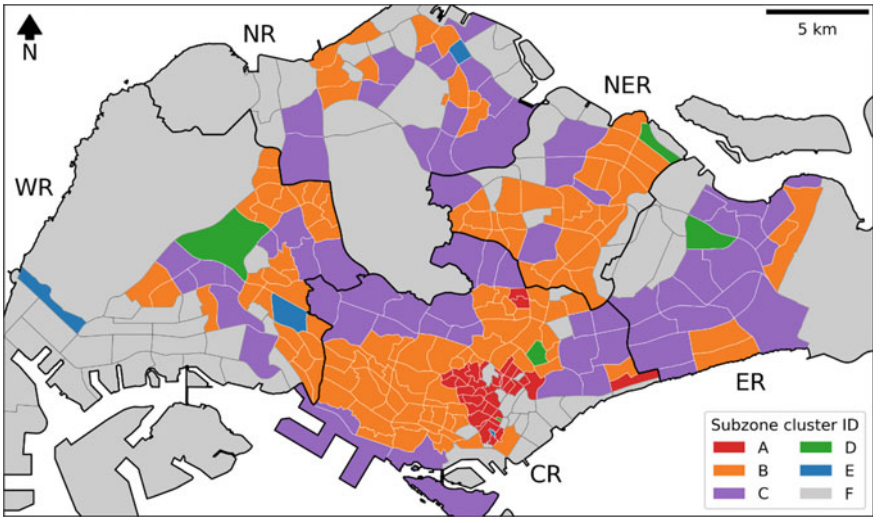

Fig. 6.12 Spatial distribution of the clusters. The five regions were labelled as: CR: Central Region, ER: East Region, NER: North East Region, NR: North Region, and WR: West Region

the most sensitive cluster, is concentrated in the Central Region, which contains the CBD. These are places where movement should be restricted to less than 100 m to achieve the reduced IV. This is followed by subzones in cluster-B, where movement should be restricted to no more than 500 m, and lastly for subzones in cluster-C indicated that the IV would increase unless movement distance is restricted to less than 1 km.

6.5 Discussion

This study examines spatiotemporal vulnerability through a socio-ecological lens, considering a subzone's population density (i.e., densely populated districts are considered more vulnerable), residents' age profiles (i.e., higher proportion of young and elderly residents are more vulnerable), socio-economic conditions (i.e., higher housing resale prices as surrogate measure of higher status), proximity to POIs linked to COVID-19 infections (e.g., supermarkets, wet markets, shopping malls, and train and bus stations), land use diversity (i.e., more diverse land use associated with greater social interactions), and population activity intensity (i.e., number of commuters passing through each subzone, where more intense activities are linked to greater vulnerability).

While a static perspective to assess spatial vulnerability is well documented in the empirical literature (e.g., CDC's Social Vulnerability Index), the impact from the temporal dynamics is less established. The COVID-19 epidemic provided the opportunity to study population movement in a period of disruptions, and the factors that underscore vulnerability to disease transmissions. Specifically, the CB (i.e., lockdown) that was implemented as part of the health preventive measures to contain the outbreak created the perfect chance to scrutinize geographical regions (i.e., subzones) that are differentially exposed to the risk factors as a function of time and space.

6.5.1 Spatiotemporal Distribution of IV

Spatiotemporal vulnerability incorporates impact of local attributes (e.g., proportion of young and elderly residents who are most at risk, proximity to POI's known for infections) and the spatial lag effects. Locale vulnerability is not only affected by local risks, but also its neighboring's risk and vulnerability, including the population distributions of various age groups in the region.

In line with observations in Fig. 6.6, static, local risk factors do not change over time. However, as a result of the CB in April and May, the reduction in movement has transformed spatiotemporal vulnerability (Fig. 6.7)—all but a handful of locations have demonstrated reduced vulnerability. The subzones that reported consistent IV over the CB period include Lorong 8 Toa Payoh, Pei Chun, Farrer Park, Victoria, and Bugis. The last three subzones are part of or closest to the CBD, and thus the

result was unsurprising. However, the comparatively higher vulnerability reported in Lorong 8 Toa Payoh and Pei Chun were unexpected. The two subzones are home to plots of public houses, vehicle depots for buses and taxis, and industrial parks. A closer examination on the two subzones reveals that they are bounded by two busy highways on the North and the East (Fig. 6.13), and this greatly limits the accessibility, mobility, and exposure of residents in the two neighborhoods. The two highways are barricaded, and the flow in and out of the two subzones are restricted to the South and the West ends. As such, the elevated IV in these two areas could have been a reflection on urban spatial bottleneck. This conjecture evidently warrants further studies.

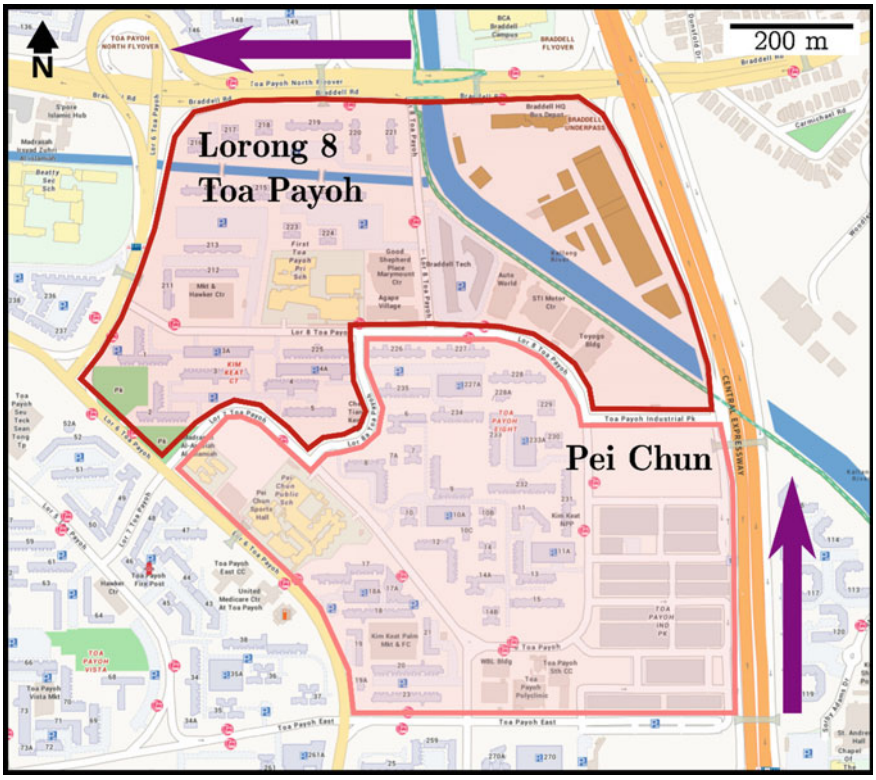

Fig. 6.13 Spatial layout of Lorong 8 Toa Payoh (boundary in red) and Pei Chun (boundary in pink) subzones, extracted from OneMap (location: 1.339 N, 103.858E, accessed: December 21, 2020, https://www.onemap.sg/main/v2/). The purple arrows show the two highways that locked in the two subzones to a corner. The blue line is a canal, with industrial buildings located on both sides

6.5.2 *Differential Impact of Mobility Distance and Circuit Breaker*

Using sensitivity analyses (Fig. 6.8), we identified distinct clusters of subzones according to their changes on the IV over a six-month period. Some subzones in the Central Region remain on the top of the IV alert list throughout the months of April and May (Fig. 6.9). In other words, reducing movement distance may not be as effective for some subzones. The results suggest that these areas could receive more epidemiological attention during the CB.

Subzones in cluster A (Fig. 6.12) show increase in IV within a shorter distance range (100–500 m) compared to subzones that are further away from the CBD and Central Region. These areas have higher spatiotemporal vulnerability, ostensibly due to the locale centrality, locations of various key administrative buildings (e.g., Immigration and Checkpoint Authority), retail and business districts (e.g., Orchard Road shopping malls, Clarke Quay and Robertson Quay), recreational facilities (e.g., East Coast Park), and transportation nodes (e.g., vehicle depots and maintenance hub for buses and taxis). Safe distancing and other health preventive measures can be strengthened and actively enforced in these areas.

Lastly, and in line with the geographic distributions of IV (Fig. 6.7), two subzones consistently show elevated risk, namely Lorong 8 Toa Payoh and Pei Chun (Fig. 6.12). The two estates are home to an estimate population of 7,160 and 10,360, respectively (Singapore Department of Statistics (n.d.)). Both neighborhoods offer a wide range of amenities and industrial land use. The IV index on Lorong 8 Toa Payoh has also remained stable overtime in-spite of the CB in April and May (Fig. 6.9). This further underscores the need for policy calibration and intervention at the local level. It should be noted that the two subzones are not the only estates with diverse, industrial land use. Whether higher IV is a result of the unusual landlock illustrated in Fig. 6.13 needs to be verified.

6.5.3 *Differential Impact of Spatial Lag Effects*

As the young and elderly residents were confined at home during CB, their distance mobility range was curtailed. However, this is not so for the working adults, some of whom were still required to travel to work. Consequently, the distance mobility for the latter group would expose the former (i.e., young, elderly) to greater epidemiological risk, at both the local and neighborhood level. The increased in IV on the young and elderly groups became obvious when the local effect was set as 0.5 (i.e., similar impact from local and regional demographic attributes) and where the distance mobility range for working adults was at least 500 m or more (Fig. 6.10).

Additionally, sensitivity analyses based on restriction of distance movement and proportion of various age demography found that as spatial lag effect increases (i.e., p reduces to 0, neighboring regions become more influential on vulnerability), the

mobility range of young and elderly people would have an impact on IV but this increment is seemingly less than the overall impact of local effects (Fig. 6.10). The result may be attributed to the smaller proportion of young and elderly residents compared to working age adults. It may also be because the differences in local risk between age groups (e.g., the accessibility to key amenities may be less important to working age adult) were not incorporated. When local effect is set to 1.0 (Fig. 6.10e), i.e., effect from neighboring region is zero and vulnerability is entirely local, the IV is fixed on the same value, and the distance for both adult and young/elderly would not have any effect.

6.6 Conclusions and Future Work

This is an exploratory study to integrate spatial and temporal information using urban public transportation data to inform and develop a measure on epidemic vulnerability. To the best of our knowledge, this study is the first of its kind and will bridge an important conceptual vacuum in Singapore, one of the most densely populated city-states in the world. Notwithstanding, there are a few methodological limitations that warrant further investigation. First, we combined and analysed six months of static human mobility data across 323 subzones. The period could be extended before and after the CB for at least a year. The additional data would allow us to simulate spatial and temporal models simultaneously, and help identify potential interactions between the two components. Comparisons between pre- and post-CB will give further insights on the efficacy of the movement restrictions.

Second, the IV model is based on various assumptions about the demographic profiles of subzones and the characteristics believed to be vulnerable to COVID-19 transmission, e.g., elderly residents as a more vulnerable group. The model's predictive validity however needs to be established and benchmarked against actual infection cases in each subzone, similar to the CDC's Social Vulnerability Index. The framework to include varying age groups for different spatial lag effects can be extended to other types of population categories, e.g., ethnicity, gender, socio-economic/education status because different categories of people might have contributed to different spatial lag effects. Future studies can explore the effect of these categories.

Taking an overarching view, the results suggest that spatiotemporal vulnerability could be shaped by multiple forces, which include the urban social and built environment, local demographic characteristics, and the composite spatial lag effects from contiguous subzones. The lockdown period in April and May provided a natural "treatment" manipulation, where we observe changes in actual mobility that result from movement restrictions. Using GIS, sensitivity tests, subgroup and cluster analyses, the findings gave us an invaluable opportunity to study this naturalistic change on spatiotemporal risk. This study has set the stage and inspired researchers to experiment with more robust and bolder methods in future endeavours.

With no end in sight for the COVID-19 pandemic, the health advisories and movement restrictions are likely to remain status quo for another year, and in turn, reinforce the work-from-home arrangement, and curate a new consumption pattern and transport utilization. The disruptions and the macro-economic forces will catalyst a decentralization trend, where residents make fewer trips to the CBD area, but more activities and movement within their neighborhood town networks (Zhong et al. 2014). This would herald a new routine and augment the importance of mobility distance and spatial lag effects.

Acknowledgements The preparation of this manuscript by the second author was supported by Singapore University of Technology and Design (Cities Sector: PIE-SGP-CTRS-1803).

Supplementary Figures

See Fig. S1.

See Fig. S2.

See Fig. S3.

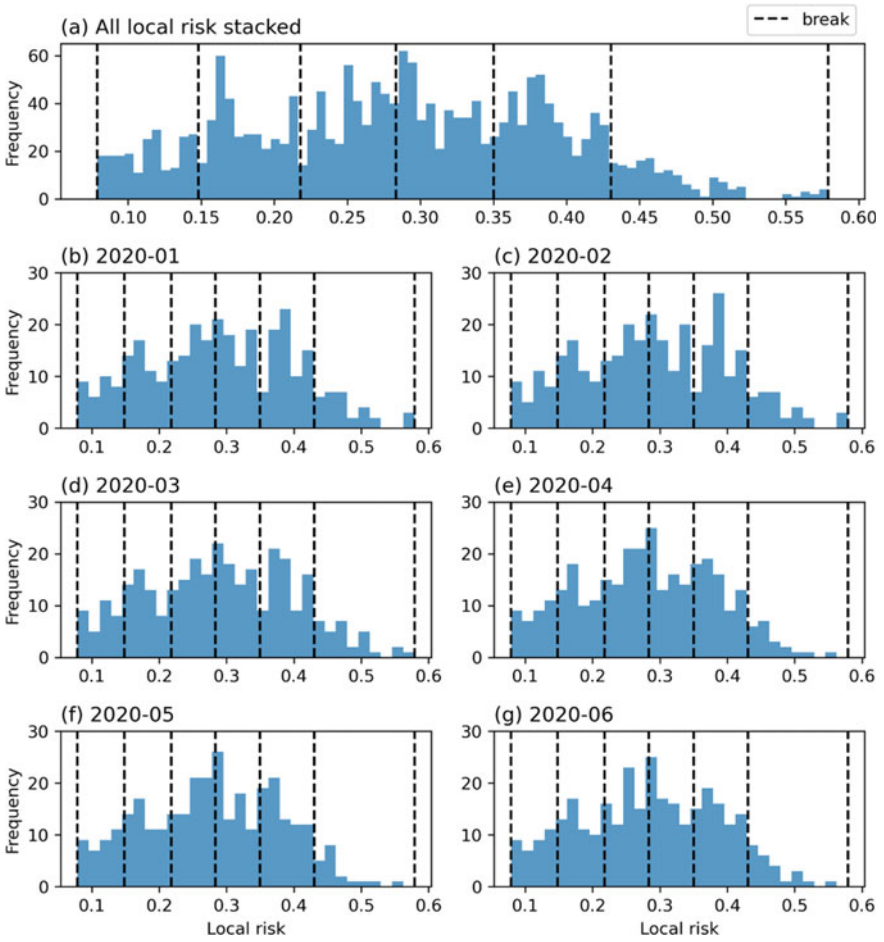

Figure S1 The histograms of: **a** all local vulnerability values, **b–g** the local vulnerability values for each month from January to June. All seven sub-plots shared the same set of Jenk's natural breaks that was calculated based on all local vulnerability values. Jenk's natural breaks method would generate breaks that aims to minimize the variance within group and maximize the variance between groups. As a result, all the five breaks (excluding the minimum and maximum values) located at the lower point (valley) in the histogram presented in (**a**). We generated Jenk's natural breaks on all local vulnerability values so that the six months shared the same set of break values, and thus the results in different months can be compared

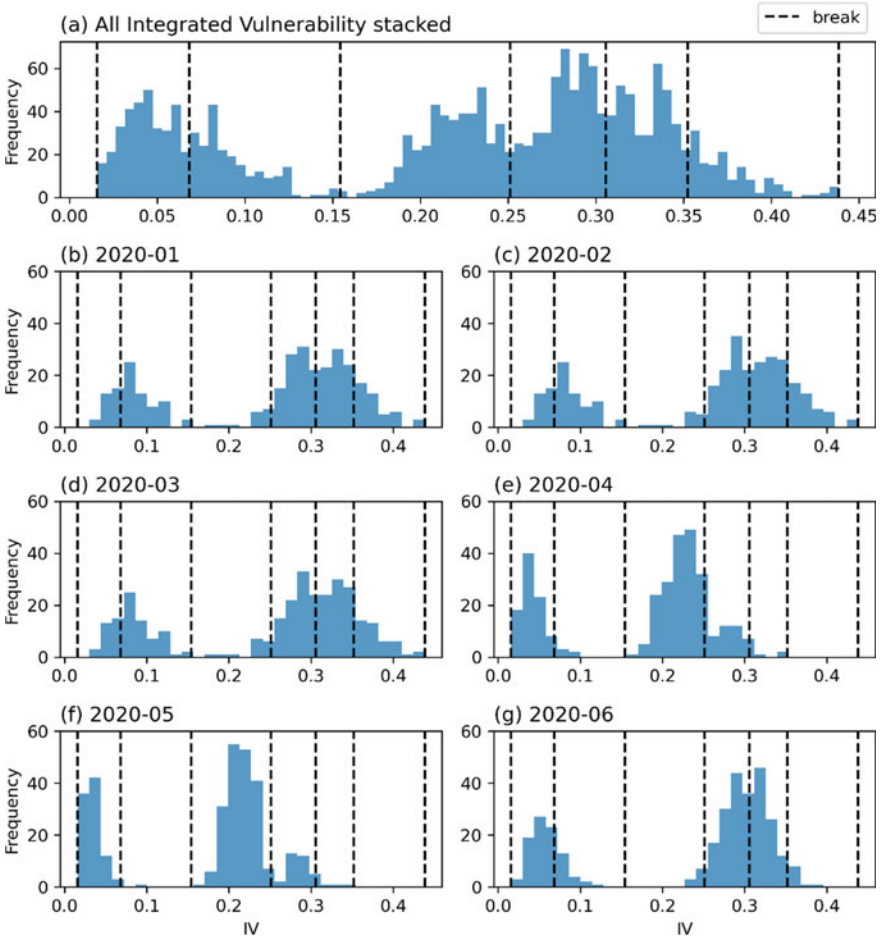

Figure S2 The histograms of: **a** all IV, **b–g** the IV for each month from January to June. All seven sub-plots shared the same set of Jenk's natural breaks that was calculated based on all IV. Similar to Figure S1, the Jenk's natural break values located at the lower points in (**a**). We generated Jenk's natural breaks on all IV so that the six months shared the same set of break values, and thus the results in different months can be compared

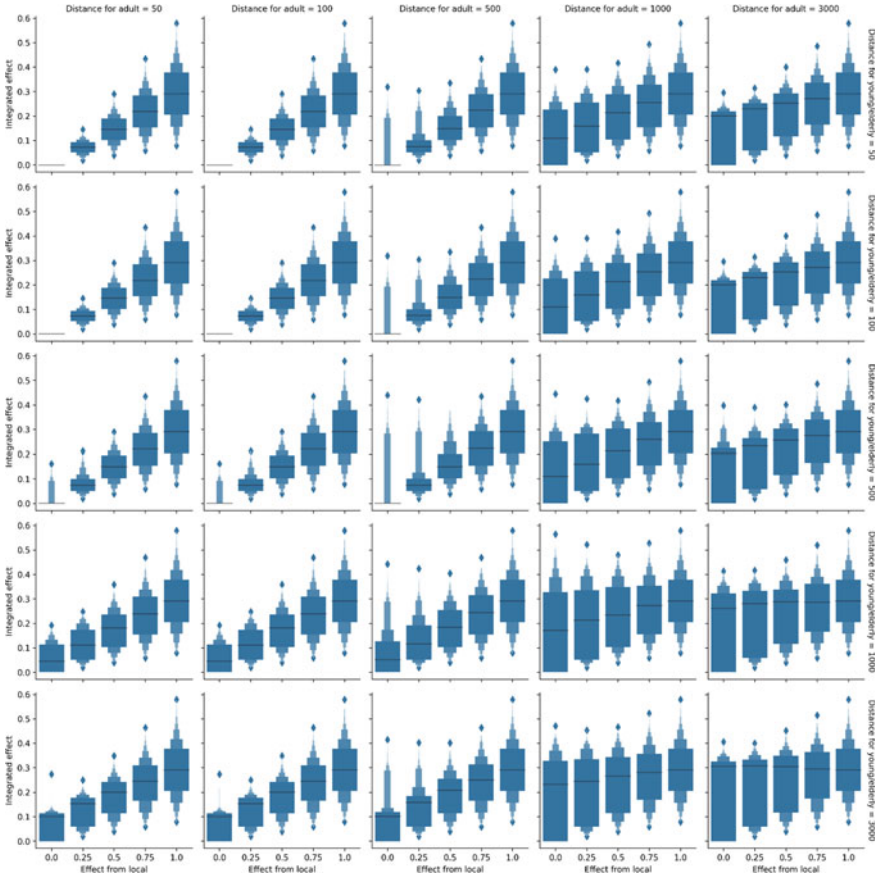

Figure S3 The boxenplot of the integrated vulnerability for each parameter combination set

References

Adger, W. N. (2006). Vulnerability. *Global Environmental Change, 16,* 268–281. https://doi.org/10.1016/j.gloenvcha.2006.02.006.

Bogich, T. L., Funk, S., Malcolm, T. R., Chhun, N., Epstein, J. H., Chmura, A. A., et al. (2013). Using network theory to identify the causes of disease outbreaks of unknown origin. *Journal of the Royal Society, Interface, 10,* 20120904.

Bratman, G. N., Hamilton, J. P., & Daily, G. C. (2012). The impacts of nature experience on human cognitive function and mental health. *Annals of the New York Academy of Sciences, 1249,* 118–136. https://doi.org/10.1111/j.1749-6632.2011.06400.x.

Chin, W. C. B., & Bouffanais, R. (2020). Spatial super-spreaders and super-susceptibles in human movement networks. *Scientific Reports, 10,* 18642. https://doi.org/10.1038/s41598-020-75697-z.

Cutter, S. L. (1996). Vulnerability to environmental hazards. *Progress in Human Geography*, *20*(4), 529–39. https://doi.org/10.1177/2F030913259602000407.

Cutter, S. L., Boruff, B. J., & Shirley, W. L. (2003). Social vulnerability to environmental hazards. *Social Science Quarterly, 84*(2), 242–261. https://doi.org/10.1111/1540-6237.8402002.

Cutter, S. L., Barnes, L., Berry, M., Burton, C., Evans, E., Tate, E., et al. (2008). A place-based model for understanding community resilience. *Global Environmental Change, 18,* 598–606. https://doi.org/10.1016/j.gloenvcha.2008.07.013.

Flanagan, B., Hallisey, E., Adams, E., & Lavery, A. (2018). Measuring community vulnerability to natural and anthropogenic hazards: The centers for disease control and prevention's social vulnerability index. *Journal of Environmental Health, 80,* 34–36.

Gómez, J., & Verdú, M. (2017). Network theory may explain the vulnerability of medieval human settlements to the Black Death pandemic. *Scientific Reports, 7,* 43467. https://doi.org/10.1038/srep43467.

Huang, C. Y., Chin, W. C. B., Wen, T. H., Fu, Y. H., & Tsai, Y. S. (2019). Epirank: Modeling bidirectional disease spread in asymmetric commuting networks. *Scientific reports, 9*(1), 1–15. https://doi.org/10.1038/s41598-019-41719-8.

Karaye, I. M., & Horney, J. A. (2020). The Impact of Social Vulnerability on COVID-19 in the U.S.: An analysis of spatially varying relationships. *American Journal of Preventive Medicine, 59*(3), 317–325. https://doi.org/10.1016/j.amepre.2020.06.006.

Lehnert, E. A., Wilt, G., Flanagan, B., & Hallisey, E. (2020). Spatial exploration of the CDC's social vulnerability index and heat-related health outcomes in Georgia. *International Journal of Disaster Risk Reduction, 46,*. https://doi.org/10.1016/j.ijdrr.2020.101517.

Leslie, E., Coffee, N., Frank, L., Owen, N., Bauman, A., & Hugo, G. (2007). Walkability of local communities: Using geographic information systems to objectively assess relevant environmental attributes. *Health and Place, 13*(1), 111–122. https://doi.org/10.1016/j.healthplace.2005.11.001.

Lewis, D. (2020). Coronavirus in the air. *Nature, 583,* 510–513.

McMahana, E. A., & Estesb, D. (2015). The effect of contact with natural environments on positive and negative affect: A meta-analysis. *Journal of Positive Psychology, 10*(6), 507–519. https://doi.org/10.1080/17439760.2014.994224.

Ministry of Health (n.d.). Updates on COVID-19 (Coronavirus disease 2019) local situation. Retrieved July 31, 2020 at https://www.moh.gov.sg/covid-19.

Morawska, L., & Milton, D. K. (2020). It is time to address airborne transmission of COVID-19. *Clinical Infectious Diseases*, ciaa939. https://doi.org/10.1093/cid/ciaa939.

Mueller, A. L., McNamara, M. S., & Sinclair, D. A. (2020). Why does COVID-19 disproportionately affect older people? *Aging*, *12*(10), 9959–9981. https://doi.org/10.18632/aging.103344.

Nayak, A., Islam, S. J., Mehta, A., Ko, Y. A., Patel, S. A., Goyal, A., et al. (2020). Impact of social vulnerability on COVID-19 incidence and outcomes in the United States. *MedRxiv*. https://doi.org/10.1101/2020.04.10.20060962.

Petrosillo, N., Viceconte, G., Ergonul, O., Ippolito, G., & Petersen, E. (2020). COVID-19, SARS and MERS: Are they closely related? *Clinical Microbiology & Infection, 26*(6), 729–734. https://doi.org/10.1016/j.cmi.2020.03.026.

Rufat, S., Tate, E., Burton, C. G., & Maroof, A. S. (2015). Social vulnerability to floods: Review of case studies and implications for measurement. *International Journal of Disaster Risk Reduction, 14*(4), 470–486. https://doi.org/10.1016/j.ijdrr.2015.09.013.

Schmidtlein, M. C., Shafer, J. M., Berry, M., & Cutter, S. L. (2011). Modeled earthquake losses and social vulnerability in Charleston, South Carolina. *Applied Geography, 31*(1), 269–281. https://doi.org/10.1016/j.apgeog.2010.06.001.

Schwirtz, M., & Cook, L. R. (2020). These N.Y.C. neighborhoods have the highest rates of virus death. *The New York Times.* Retrieved May 19, 2020, at https://www.nytimes.com/2020/05/18/nyregion/coronavirus-deaths-nyc.html.

Shannon, C. (1948). A mathematical theory of communication. *Bell System Technical Journal, 27*(4), 623–656.

Singapore Department of Statistics (n.d.). Geographic distribution. Retrieved Nov 25, 2020, at https://www.singstat.gov.sg/find-data/search-by-theme/population/geographic-distribution/latest-data.

Snyder, B., & Parks, V. (2020). Spatial variation in socio-ecological vulnerability to COVID-19 in the contiguous United States. Retrieved May 19, 2020 http://doi.org/10.2139/ssrn.3587713.

Tatem, A. J., Rogers, D. J., & Hay, S. I. (2006). Global transport networks and infectious disease spread. *Advances in Parasitology, 62,* 293–343. https://doi.org/10.1016/S0065-308X(05)62009-X.

Yonker, L. M., Neilan, A. M., Bartsch, Y., Patel, A. B., Regan, J., Arya, P., et al. (2020). A.Pediatric severe acute respiratory syndrome coronavirus 2 (SARS-COV-2): Clinical presentation, infectivity, and immune responses. *Journal of Pediatrics, 227,* 45–52. https://doi.org/10.1016/j.jpeds.2020.08.037.

Zhong, C., Arisona, S. M., Huang, X., Batty, M., & Schmitt, C. (2014). Detecting the dynamics of urban structure through spatial network analysis. *International Journal of Geographical Information Science, 28*(11), 2178–2199. https://doi.org/10.1080/13658816.2014.914521.